Cellular/Molecular

Ca^{2+}–Calmodulin Feedback Mediates Sensory Adaptation and Inhibits Pheromone-Sensitive Ion Channels in the Vomeronasal Organ

Jennifer Spehr,[1] Silke Hagendorf,[2] Jan Weiss,[3] Marc Spehr,[2] Trese Leinders-Zufall,[3] and Frank Zufall[3]

[1]Department of Cellular Physiology and [2]Emmy Noether Research Group, Ruhr University of Bochum, 44780 Bochum, Germany, and [3]Department of Physiology, University of Saarland School of Medicine, 66421 Homburg, Germany

The mammalian vomeronasal organ (VNO) mediates the regulation of social behaviors by complex chemical signals. These cues trigger transient elevations of intracellular Ca^{2+} in vomeronasal sensory neurons (VSNs), but the functional role of such Ca^{2+} elevations is unknown. We show that stimulus-induced Ca^{2+} entry plays an essential role as a negative feedback regulator of VSN sensitivity. Electrophysiological VSN responses undergo effective sensory adaptation that requires the influx of Ca^{2+} and is mediated by calmodulin (CaM). Removal of the Ca^{2+}–CaM feedback eliminates this form of adaptation. A key target of this feedback module is the pheromone-sensitive TRPC2-dependent cation channel of VSNs, as its activation is strongly inhibited by Ca^{2+}–CaM. Our results reveal a previously unrecognized CaM-signaling pathway that endows the VSNs with a mechanism for adjusting gain and sensitivity of chemosensory signaling in the VNO.

Key words: **pheromone sensing; modulation; Ca^{2+} feedback; TRPC2; gain control; olfactory**

Introduction

The murine vomeronasal organ (VNO) plays an essential role in the detection of complex chemical cues that regulate a wide variety of social behaviors including male–male territorial aggression, maternal aggression, mating, and individual recognition (Meredith, 1983; Wysocki and Lepri, 1991; Del Punta et al., 2002; Leypold et al., 2002; Stowers et al., 2002; Kimchi et al., 2007). The ability of the VNO to orchestrate such behaviors depends critically on the proper functioning of almost half a million vomeronasal sensory neurons (VSNs) residing in the organ. VSNs are among the most sensitive chemodetectors in mammals, with activation thresholds in the picomolar range, and their responses saturate over ~2–3 orders of magnitude of ligand concentration, indicating that these neurons are capable of encoding stimulus intensity over a given concentration range (Leinders-Zufall et al., 2000, 2004; Kimoto et al., 2005). Stimulus-induced VSN responses appear to be mediated by the activity of a phospholipase C-signaling cascade (Holy et al., 2000; Lucas et al., 2003) that causes the opening of Ca^{2+}-permeable cation channels and ultimately leads to Ca^{2+} entry and elevation of intracellular Ca^{2+} (for review, see Zufall et al., 2005). The transient receptor potential channel TRPC2 is essential for this cellular response (Liman et al., 1999; Leypold et al., 2002; Stowers et al., 2002; Lucas et al., 2003). Although this receptor-induced Ca^{2+} signal has been used widely to monitor VSN response properties (Leinders-Zufall et al., 2000, 2004; Cinelli et al., 2002; Spehr et al., 2002; Chamero et al., 2007; He et al., 2008), the biological role of the Ca^{2+} rise remains unknown. Here, we begin to define the role of Ca^{2+} signaling in native vomeronasal function by asking the following: (1) Is the stimulus-induced Ca^{2+} rise part of a regulatory feedback mechanism that modulates VSN responsivity and thus could mediate cellular adaptation and sensitivity regulation? (2) If so, is the Ca^{2+} sensor calmodulin (CaM) involved in the feedback loop? (3) Are the pheromone-sensitive ion channels a substantial target for Ca^{2+}–CaM-mediated feedback regulation?

Materials and Methods

Animals. Experiments were performed on 30- to 90-d-old C67BL6 mice (either sex). The relevant Institutional Animal Care and Use Committees approved all procedures.

Inside-out patch-clamp recordings. Freshly dissociated VSNs were prepared as described previously (Lucas et al., 2003). Inside-out patch-clamp recordings closely followed previously described procedures (Lucas et al., 2003). Isolated membrane patches excised from the dendritic tip of a VSN were transferred to a separate chamber (Warner Instruments) that permitted exchange of the solution surrounding the membrane patch without contamination of the cell population. Standard pipette and bath (intracellular) solutions in inside-out experiments consisted of the following (in mM): 140 NaCl, 10 Na-HEPES, 1 EGTA, pH 7.1 (HCl), adjusted to 300 mOsm (glucose). For experiments using a free Ca^{2+} concentration of 50 μM, we used the following (in mM): 140 NaCl, 2 nitriloacetic acid (Na^+ salt), 0.39 $CaCl_2$, 10 Na-HEPES, pH 7.1, adjusted to 300 mOsm (glucose). The same solutions were used for the analysis of Ca^{2+}-activated channels in inside-out experiments. In some

Received Nov. 10, 2008; revised Jan. 9, 2009; accepted Jan. 11, 2009.

This work was supported by Deutsche Forschungsgemeinschaft Grants Sonderforschungsbereich 530/A7 (to F.Z.) and SP 939/1-1 (to J.S.), and by the Emmy Noether Program (SP724/2-1) of the Deutsche Forschungsgemeinschaft (to M.S.). T.L.-Z. is a Lichtenberg Professor of the Volkswagen Foundation. We thank Andrew Lane and Kirill Ukhanov for assistance in early stages of this project and Emily Liman for providing anti-TRPC2 antibodies.

Correspondence should be addressed to Frank Zufall, Department of Physiology, University of Saarland School of Medicine, Building 58, 66421 Homburg, Germany. E-mail: frank.zufall@uks.eu.

DOI:10.1523/JNEUROSCI.5416-08.2009

 0270-6474/09/292125-11$15.00/0

experiments, we used an intracellular solution that contained 50 μM Ca^{2+} but reduced Na^+ and Cl^- concentrations (in mM): 14 NaCl, 2 nitriloacetic acid (Na^+ salt), 0.39 $CaCl_2$, 10 Na-HEPES, pH 7.1, adjusted to 300 mOsm (glucose). Free Ca^{2+} concentrations were calculated using WEBMAXC STANDARD (www.stanford.edu/~cpatton/maxc.html). An EPC-9 patch-clamp amplifier (Heka Electronics) was used for all recordings, command potential sequences, data acquisition and online analyses. Inside-out experiments usually were performed at a membrane potential of −20 mV and voltage ramps (duration 100 ms, slope −1.6 mV/ms) were applied every 5 s. If not otherwise stated, leak conductance was measured immediately before application of 1-stearoyl-2-arachidonoyl-*sn*-glycerol (SAG) and subtracted digitally from original current–voltage (*I–V*) curves during off-line analysis. Experiments shown in Figure 1, *C* and *D*, are original data without any leak subtraction. For solution exchange, patches were positioned in front of two glass pipettes, each connected to a reservoir. Solution exchange was achieved by moving the electrode from one stream to another (flow rate, ~400 μl/min). At the beginning of an experiment, patches were exposed for at least 3 min to Ca^{2+}-buffered standard intracellular solution before CaM was applied. During this time baseline conditions were recorded, each patch was tested briefly for the presence of Ca^{2+}-activated channels, and the TRPC2-dependent channels were activated.

Whole-cell patch-clamp recordings. Whole-cell recordings from individual VSNs were obtained in acute VNO tissue slices (Lucas et al., 2003; Ukhanov et al., 2007). The VNO was embedded in 4% low-gelling temperature agarose, and coronal slices (300 μm) were cut on a vibratome (VT1000S; Leica Microsystems). Slices were transferred to a submerged, chilled, and oxygenated storage chamber until use. The following solutions were used. (1) HEPES-buffered extracellular solution containing (in mM) 145 NaCl, 5 KCl, 1 $CaCl_2$, 1 $MgCl_2$, 10 HEPES; pH = 7.3 (adjusted with NaOH); osmolarity = 300 mOsm (adjusted with glucose). (2) Bicarbonate-buffered oxygenated (95% O_2/5% CO_2) extracellular solution containing (in mM) 120 NaCl, 25 $NaHCO_3$, 5 KCl, 1 $MgSO_4$, 1 $CaCl_2$, 5 BES (*N*,*N*-bis[2-hydroxyethyl]-2-aminoethansulfonic acid); pH = 7.3; osmolarity = 300 mOsm. (3) HEPES-buffered pipette solution containing (in mM) 143 KCl, 10 HEPES, 2 KOH, 0.3 $CaCl_2$, 1 EGTA (110 nM free Ca^{2+}), 1 MgATP, 0.5 NaGTP, pH = 7.1 (adjusted with KOH); osmolarity = 290 mOsm. If not stated otherwise, all chemicals were purchased from Sigma. Individual VSNs were visualized using a Leica DM LFSA (Leica Microsystems) fixed-stage microscope equipped with infrared-optimized differential interference contrast optics. Slices were continuously superfused with oxygenated extracellular solution (~3 ml/min; gravity flow) at room temperature. Patch pipettes (5–7 MΩ) were pulled from borosilicate glass capillaries with filament (1.50 mm OD/0.86 mm ID; Science Products) on a PC-10 vertical micropipette puller (Narishige Instruments) and fire polished using a MF-830 Microforge (Narishige Instruments). An EPC-10 amplifier controlled by Patchmaster 2.32 software (HEKA Elektronik) was used for data acquisition. Focal stimulus and ophiobolin A application was achieved by a custom-made, pressure-driven application device. CALP2 was included in the intracellular solution and applied via the patch pipette. In current-clamp experiments, after break-in, the membrane potential was set to −75 mV by injecting a constant holding current (≤ ±3 pA). Action potential discharge in response to either diluted urine (1:100) or depolarizing current injections (2 pA) was monitored at a sampling rate of 10 kHz. Stimuli were applied twice for 20 s with an interstimulus interval of 30 s. Signals were low-pass filtered (analog 3- and 4-pole Bessel filters in series) with an effective corner frequency (−3 dB) of 2.9 kHz.

Field potential recordings. Stimulus-evoked local field potentials were recorded from the luminal surface of intact VNO sensory epithelia as

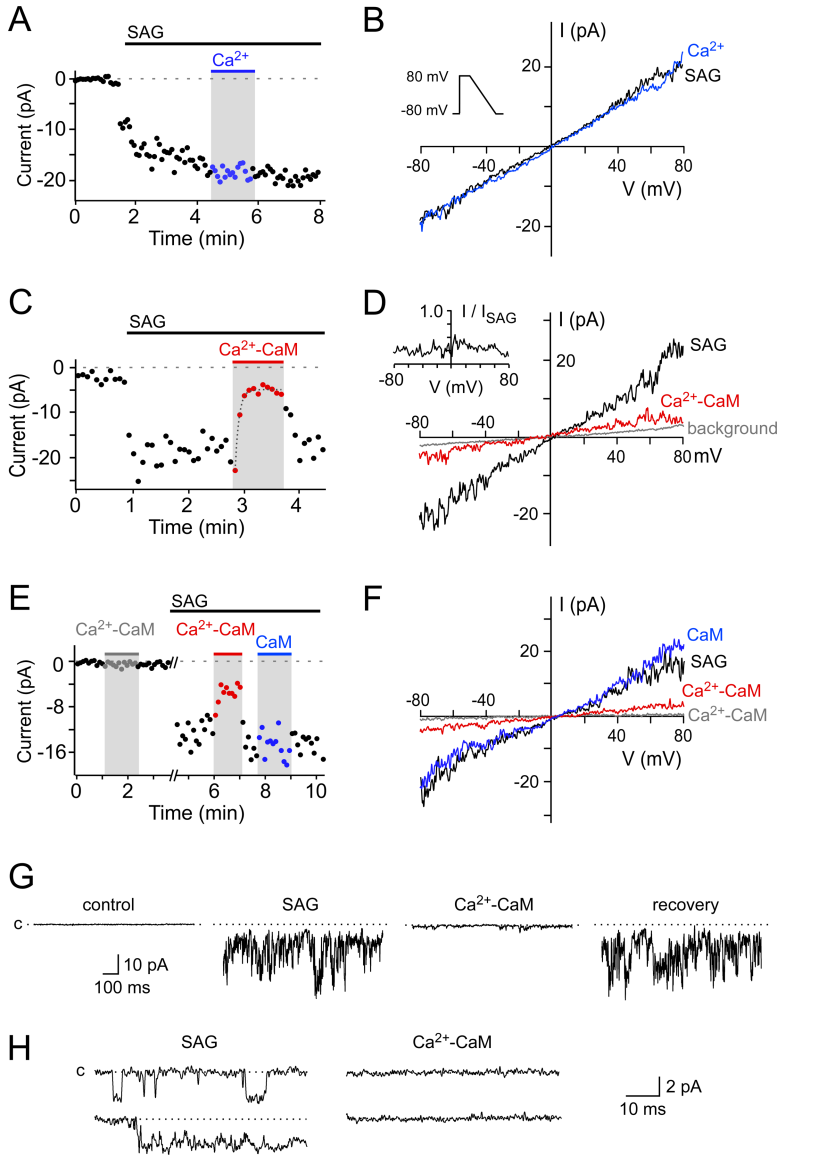

Figure 1. Native TRPC2-dependent cation channels from mouse VSN dendrites are inhibited by Ca^{2+}–CaM. ***A***, SAG-induced currents plotted over time. Each dot represents the current at −70 mV obtained from individual voltage ramps as in ***B***. SAG concentration, 30 μM. Application of 50 μM Ca^{2+} (blue) to the intracellular membrane face is without effect. ***B***, *I–V* relationship of SAG-induced conductance measured under control conditions (control, black) and with 50 μM intracellular Ca^{2+} (blue). Curves were elicited by voltage ramps as indicated. ***C***, ***D***, Effect of Ca^{2+}–CaM (red; 1 μM CaM, 50 μM Ca^{2+}) on the SAG conductance. Dotted line in ***C*** is a single exponential fit of the onset time course of Ca^{2+}–CaM-mediated channel inhibition. Background conductance (gray) was measured before SAG application. Inset in ***D*** indicates that the extent of the Ca^{2+}–CaM effect is voltage independent between −80 mV and +80 mV ($I_{Ca2+\text{-}CaM}/I_{SAG}$). ***E***, ***F***, Ca^{2+}–CaM (red) but not CaM applied by itself (1 μM, blue) inhibits the SAG conductance. Note that Ca^{2+}–CaM has no effect on the background conductance (gray). ***G***, Sustained SAG-induced channel activity at fixed membrane potential (−70 mV) is reversibly inhibited by Ca^{2+}–CaM application. Dotted line (c) represents zero current level. ***H***, Examples of single-channel events evoked by the continuous application of SAG (20 μM). Holding potential, −70 mV. Channel activity is suppressed during Ca^{2+}–CaM application (1 μM CaM, 50 μM Ca^{2+}). Bandwidth, 0–2.0 kHz.

described and chemical stimuli were focally ejected onto VSN microvilli using multibarrelled stimulation pipettes (Leinders-Zufall et al., 2000, 2004; Leypold et al., 2002; Del Punta et al., 2002).

Chemicals. Stock solutions of SAG (Calbiochem) were prepared in DMSO and aliquots stored at −20°C. Final solutions were made immediately before use, briefly sonicated, and directly added to the recording chamber (Lucas et al., 2003). CaM (Sigma), ophiobolin A (Alexis), CALP2 (Tocris) and autocamtide-2 related inhibitory peptide-II (Calbiochem) were applied via microperfusion. Stock solutions of CaM were prepared in distilled water and maximally stored for 1 week. Stock solutions of ophiobolin A were prepared using chloroform, immediately diluted in DMSO and stored at −20°C. CALP2 was prepared freshly in DMSO/MeOH (1:1). Final DMSO concentrations used (≤0.1%) were also tested alone in controls and had no effect. Fresh urine, a rich source of natural pheromones, was collected daily from male or female mice and diluted 1:1000 or 1:100 before use.

Immunohistochemistry. For immunohistochemical analysis of VNO sections, the VNO was dissected as described previously (Leinders-Zufall et al. 2004) and fixed for 2 h in 4% paraformaldehyde (in PBS) at 4°C, decalcified overnight in 0.5 M EDTA and cryoprotected in PBS containing 30% sucrose. The dehydrated VNO was embedded in Tissue Freezing Medium and sectioned at 25 μm on a cryostat (Leica Microsystems). Blocking was performed for 1 h in PBS containing 2% goat serum, 1% gelatin and 0.2% Triton X-100 (blocking solution). Sections were then incubated overnight (4°C) in blocking solution containing polyclonal rabbit anti-CaM (1:100; Zymed Laboratories) and anti-TRPC2 antibodies (1:500; kindly provided by Dr. E.R. Liman, University of Southern California, Los Angeles, CA), respectively (Liman et al., 1999). After washing in PBS containing 0.05% Triton X-100 (3 × 10 min, 1 × 30 min), sections were incubated for 1 h with goat anti-rabbit Alexa Fluor532 and 633 secondary antibodies (1:500; Invitrogen). Excess antibodies were removed by washing in PBS containing 0.05% Triton X-100 (3 × 10 min, 1 × 30 min). For multilabeling, we adopted a published protocol that uses Fab fragments for blocking and labeling (Leinders-Zufall et al., 2004). To control for nonspecific staining, experiments in which the primary antibodies were omitted were performed in parallel with each procedure. Dissociated VSNs were prepared as described above except that we removed nondissociated cells from the cell suspension by means of BD Falcon Cell Strainer nylon meshes (70 μm pore diameter; Becton Dickinson). Single VSNs attached to concanavalin A (Sigma) coated dishes were fixed for 30 min in 4% paraformaldehyde in PBS (4°C). VSNs were washed 3 times in PBS (10 min) and incubated at room temperature (RT, 30 min) in blocking solution. This was followed by incubation in blocking solution containing a polyclonal rabbit anti-CaM antibody (1:100; Zymed Laboratories; 1 h at RT). The cells were then washed 3 times in PBS (10 min) and incubated in blocking solution containing goat anti-rabbit Alexa Fluor633 (1:500; Invitrogen). No labeling was observed in control cells in which the primary antibody was omitted.

Fluorescent images were captured using an upright scanning confocal microscope (LSM510-Meta; Zeiss) equipped with 10× (n.a. 0.30), 40× (n.a. 0.80), and 63× (n.a. 0.90) water-immersion objectives. To eliminate cross talk between labels, the multitracking configuration was applied. Endogenously expressed green fluorescent protein (GFP) was excited using the 488 nm line of an argon laser and emitted fluorescence was captured using a bandpass filter (500–550IR nm). Alexa Fluor532 and Fluor633 were excited using the 543 and 633 nm line of a helium/neon laser, respectively, and fluorescence was captured using a long-pass filter (560 nm; Alexa Fluor532) or a bandpass filter (650–710 nm; Alexa Fluor633). Digital images were uniformly adjusted for brightness and contrast using Adobe Photoshop CS3 (Adobe Systems).

Data analyses. Electrophysiological data were analyzed with FitMaster 2.20 (HEKA Elektronik) and IGOR PRO software (WaveMetrics). Statistical analysis was done with SigmaStat 3.11 (Systat Software). The Student's *t* test was used for measuring the significance of difference between two distributions. Multiple groups were compared using a one-way or two-way ANOVA. The Fisher's least significant difference (LSD) test was used as a *post hoc* comparison of the ANOVA. If not otherwise stated, data are expressed as means ± SEM.

Results

Ca^{2+}–CaM modulation of diacylglycerol-sensitive cation channels

Given that the N terminus of TRPC2 binds CaM in a Ca^{2+}-dependent manner (Yildirim et al., 2003), we reasoned that the ion channels underlying primary sensory transduction in VSNs might be a target of a Ca^{2+}-mediated negative feedback loop. To test this, we recorded native TRPC2-dependent cation channels in inside-out patches of plasma membrane excised from the dendritic tips of dissociated mouse VSNs (Lucas et al., 2003). We activated the channels by applying the diacylglycerol analog SAG (30 μM; $n = 49$) to the cytosolic membrane face of the patch and monitored the SAG conductance by measuring *I–V* curves at a rate of 0.2 Hz. With symmetrical divalent cation-free NaCl solutions, the conductance does not desensitize (Fig. 1*A*) (Lucas et al., 2003), and *I–V* curves are almost linear with a reversal potential of 0 mV (Fig. 1*B*, SAG).

When we exposed patches to a solution containing 50 μM Ca^{2+} (Fig. 1*A*,*B*), the size or shape of the SAG-activated conductance did not change noticeably; mean current amplitude at −70 mV was 102 ± 2.6% of control ($n = 6$). In contrast, when we added CaM (1 μM) together with 50 μM Ca^{2+} (Ca^{2+}–CaM), the SAG conductance was dramatically diminished (Fig. 1*C*,*D*). Under these conditions, current amplitude measured at −70 mV was reduced to 17.9 ± 4.6% of control ($n = 12$, *t* test: $p = 0.006$). This effect of Ca^{2+}–CaM was voltage-independent (Fig. 1*D*, inset) and could be reversed upon washout. The inhibitory action of Ca^{2+}–CaM on the SAG conductance occurred with an approximate time constant of 3–4 s under our conditions, as revealed from single exponential fits of the onset time course of Ca^{2+}–CaM-induced channel inhibition (Fig. 1*C*, dotted line). Subsequent application of Ca^{2+}–CaM reduced the SAG conductance to a similar extent (20.7 ± 12% of control, $n = 3$). CaM (1 μM) applied by itself without added Ca^{2+} did not produce such channel inhibition (104.7 ± 7.7% of control, $n = 3$) (Fig. 1*E*,*F*). There was no effect of Ca^{2+}–CaM on the background current measured under control conditions before SAG application (Fig. 1*E*,*F*).

To confirm that Ca^{2+}–CaM inhibited SAG-induced channel activation, currents were also measured at fixed holding potential (−70 mV; $n = 4$). In the example of Figure 1*G*, SAG caused sustained channel activity that was suppressed after application of Ca^{2+}–CaM. This inhibitory effect could be reversed upon washout of Ca^{2+}–CaM, consistent with the results obtained from ramp experiments. High resolution analysis in patches that contained only one or a very few channels ($n = 3$) confirmed that Ca^{2+}–CaM inhibits the same 42-pS SAG-sensitive cation channel that we described previously (Lucas et al., 2003) (Fig. 1*H*). Thus, together, the results of Figure 1 indicate that Ca^{2+}–CaM functions as a powerful regulator of the activity of native TRPC2-dependent cation channels from VSN dendrites.

A Ca^{2+}-activated cation conductance in mouse VSNs

In a subset of the inside-out patches (7/56, 12.5%), we found that 50 μM Ca^{2+} applied to the cytosolic membrane face causes activation of a substantial inward current at −70 mV with symmetrical NaCl solutions. A representative example is depicted in Figure 2*A–C*. The *I–V* curve of this Ca^{2+}-activated conductance displayed slightly inward rectifying properties and reversed at 0 mV. To determine whether the conductance was of cationic or anionic nature, we exposed the patch to a solution in which Na^+ and Cl^- were diluted tenfold by substitution with glucose (low NaCl) (Liman, 2003). This resulted in a reversal potential shift to

33 ± 4.5 mV ($n = 4$), close to the theoretical value of 42 mV for a cation selective conductance (Fig. 2*B*). These results confirm the existence of Ca^{2+}-activated cation (CAN) channels in dendritic knobs of mammalian VSNs (Liman, 2003) and extend the finding from hamster to mouse. All patches that showed such Ca^{2+}-activated channels were excluded from experiments in which the effect of Ca^{2+}–CaM on the SAG conductance was investigated.

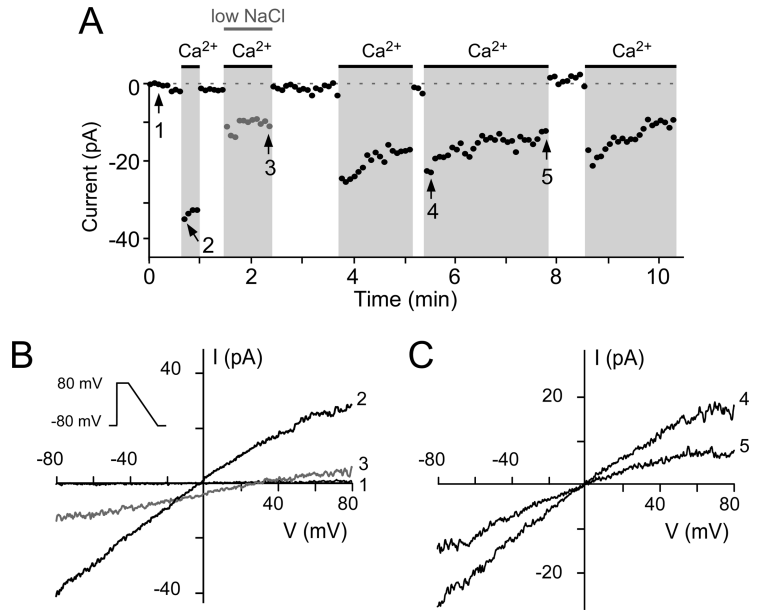

Figure 2. A Ca^{2+}-activated cation conductance exists in a subset of inside-out patches from dendritic knobs of mouse VSNs. ***A***, Plot over time of the current at −70 mV in response to repetitive voltage ramps (inset, ***B***). Repeated exposure to 50 μM Ca^{2+} results in the activation of an inward current, an effect that is reversed upon Ca^{2+} removal. The Ca^{2+}-activated current diminishes over time. ***B***, *I–V* curves of Ca^{2+}-activated conductance measured at the beginning of the experiment with symmetrical divalent cation-free NaCl solutions (trace 1) and with 50 μM Ca^{2+} (trace 2). Exposure to a 10-fold diluted intracellular solution (low NaCl) reduces the conductance (***A***, ***B***) and shifts the reversal potential from 0 to 30 mV (trace 3). ***C***, Comparison of Ca^{2+}-activated cation conductance at different times in the experiment (trace 4 and trace 5). Some run-down is evident. Time points at which original ramp currents were recorded are indicated in ***A***.

CaM localization to VSN microvilli

Since the presence of CaM in VSNs had not been reported previously, we performed an immunocytochemical analysis using an antibody directed against CaM (Fig. 3*A–E*, green). In VNO sections prepared from a gene-targeted mouse strain in which all mature VSNs can be visualized on the basis of their expression of GFP (gray) under the control of the regulatory sequences of the *omp* (olfactory marker protein) gene (Potter et al., 2001), CaM immunoreactivity was evident in virtually all VSNs including their cell bodies and dendrites (Fig. 3*A*). To determine whether CaM was also expressed in VSN microvilli, the structures that are the primary site of pheromonal signaling in the VNO, we used costaining with an antibody directed against TRPC2 (Fig. 3*B*, red) that labels primarily the sensory microvilli of VSNs (Liman et al., 1999). The merged images (Fig. 3*C*,*E*, yellow) indicate that CaM is colocalized with TRPC2 in VSN microvilli, confirming that CaM has the potential to regulate primary signal transduction in intact VSNs. Analysis of CaM immunoreactivity in single, dissociated VSNs supported this conclusion (Fig. 3*F*).

Concentration dependence of CaM-mediated channel inhibition

We next analyzed the dependence of Ca^{2+}–CaM-induced channel inhibition on CaM concentration (Fig. 4*A*). Averaged results from several experiments at −70 mV were plotted as dose–response relationship (50 μM Ca^{2+}, 30 μM SAG). A fit of the data points using the Hill equation revealed a $K_{1/2}$ value of 540 nM and a Hill coefficient of 2. If this inhibitory effect of CaM is involved in sensory adaptation of VSNs, the reduction in current amplitude should reflect a shift of the dynamic range of the SAG conductance toward higher SAG concentrations (Torre et al., 1995; Menini, 1999; Zufall and Leinders-Zufall, 2000). If so, Ca^{2+}–CaM-induced channel inhibition would be most effective with SAG concentrations near half-maximal channel activation (EC_{50}), whereas the effect should be reduced or absent when saturating SAG concentrations are used. This was indeed the case (Fig. 4*B–H*). Whereas Ca^{2+}–CaM (1 μM CaM, 50 μM Ca^{2+}) produced nearly complete inhibition when the channels were activated by 15 or 30 μM SAG (Fig. 4*B*,*C*), there was almost no effect when we used 100 μM SAG (Fig. 4*B*,*E*,*H*), which generates a saturating current in intact VSNs (Lucas et al., 2003). These results are consistent with a model in which Ca^{2+}–CaM reduces the effective affinity of SAG by acting on channel gating.

Disruption of CaM signaling

To obtain a clearer understanding of the functional role of Ca^{2+}–CaM-mediated channel inhibition in VSNs, we next sought to disrupt the CaM feedback. The experimental design we used was based on the goal to block the CaM feedback not only in excised membrane patches (Fig. 5) but also in intact VNO neuroepithelium (Figs. 6, 7). We found that the potent CaM antagonist ophiobolin A (Fig. 5*A*), a membrane-permeant phytotoxin produced by pathogenic fungi (Leung et al., 1984; Peters and Mayer, 1998; O'Connor et al., 1999; Au et al., 2000), is ideal for this approach. Ophiobolin A (20 μM) applied by itself had no effect on the resting conductance measured before SAG application (data not shown) or on the SAG-sensitive conductance (Fig. 5*B*,*C*,*H*). Ophiobolin A is known to rapidly bind to lysines 75, 77 and 148 in the calmodulin molecule and thereby inactivates the protein in an irreversible manner (Kong Au and Chow Leung, 1998). Accordingly, when we applied Ca^{2+}–CaM together with ophiobolin A, the Ca^{2+}–CaM-mediated inhibition of the SAG conductance was virtually absent ($n = 8$) (Fig. 5*D*,*E*,*H*). Another specific CaM antagonist, the 12-mer peptide CALP2 (VKFGVGFKVMVF; 50 μM) (Fig. 5*F*), which binds to the EF-hand/Ca^{2+}-binding site of CaM and thereby prevents activation by Ca^{2+} (Villain et al., 2000), showed the same effect ($n = 5$) (Fig. 5*F*,*G*,*H*). Other CaM antagonists such as calmidazolium were not used in this study because of their reported blocking effects on olfactory cyclic nucleotide-gated cation channels (Kleene, 1994).

Because odor adaptation of olfactory sensory neurons (OSNs) depends in part on Ca^{2+}–CaM-dependent protein kinase II (CaMKII) (Leinders-Zufall et al., 1999), we tested a potential role of CaMKII in CaM-regulated inhibition of the SAG conductance. However, application of a specific peptide inhibitor of CaMKII,

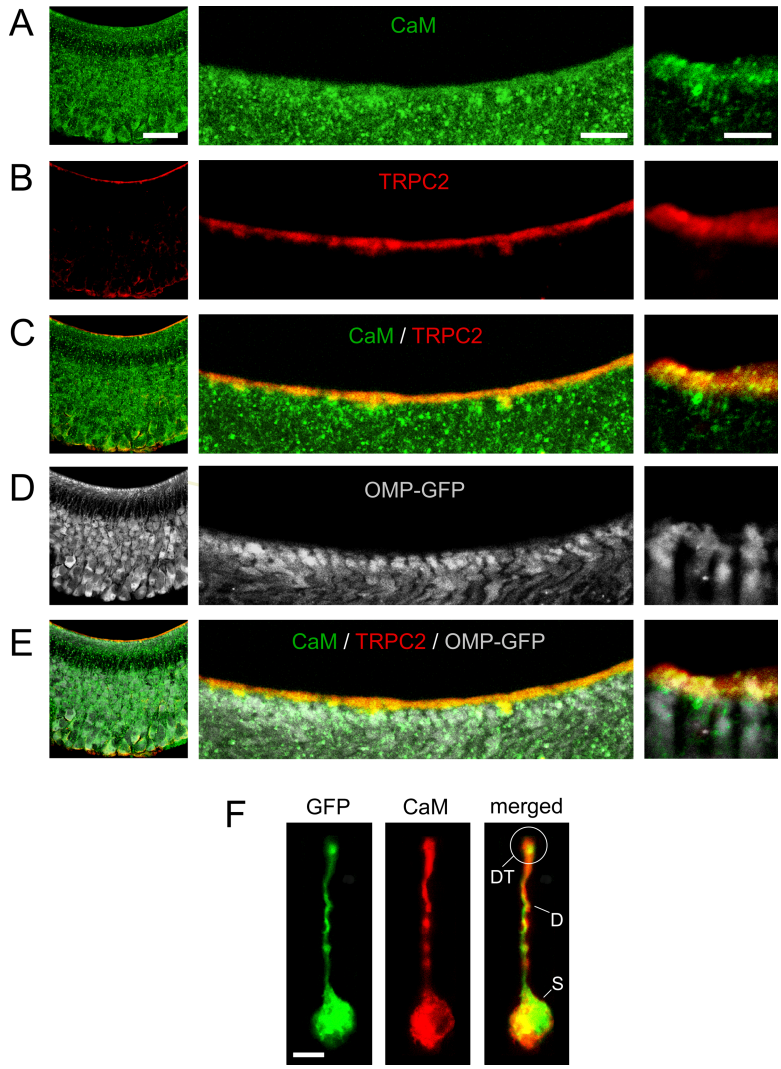

Figure 3. Localization of CaM to VSN microvilli analyzed by immunohistochemistry. ***A–E***, Confocal microscope images at low (left), intermediate (middle) and high resolution (right) show CaM (green, ***A***), TRPC2 (red, ***B***) and OMP-GFP fluorescence (gray, ***D***). Costaining of CaM and TRPC2 is observed in VSN microvilli (yellow, ***C***, ***E***). Scale bars: (left) 40 μm; (middle) 10 μm; (right) 5 μm. ***F***, CaM immunoreactivity (red) in a single, dissociated VSN. S, Soma; D, dendrite; DT, dendritic tip. Scale bar, 5 μm.

autocamtide-2 related inhibitory peptide II (AIP-II; KKKLRRQEAFDAL; 500 nM) (Ishida et al., 1998), did not prevent CaM-mediated channel inhibition, ruling out an involvement of CaMKII in this effect ($n = 4$) (Fig. 5*H*). This finding is consistent with the absence of CaMKII immunoreactivity in rodent VSNs (Menco, 2005).

VNO pheromone responses undergo Ca^{2+}–CaM-dependent sensory adaptation

Do stimulus-induced VSN responses undergo sensory adaptation? To examine this question, we first used local field potential recordings [the electro-vomeronasogram (EVG)] and measured electrophysiological responses to natural urine stimuli or single pheromone ligands from the microvillous layer of an intact VNO preparation (Leinders-Zufall et al., 2000, 2004; Del Punta et al., 2002; Leypold et al., 2002). In OSNs, odor adaptation is evident as a decrease in sensitivity arising from prolonged or previous odor exposure (Torre et al., 1995; Zufall and Leinders-Zufall, 2000; Munger et al., 2001; Song et al., 2008). We therefore applied single or paired pulses of chemostimuli. We found evidence for VSN sensory adaptation in each case (Fig. 6) ($n = 68$). For example, during prolonged stimulation with dilute urine (DU, 1:1000; 6 s), the sensory response declined in a time-dependent manner before reaching a new steady-state plateau (Fig. 6*A*,*B*). This decline in sensitivity of the VSNs followed an exponential time course with an average desensitization time constant of 2.5 ± 0.5 s ($n = 8$; range: 1.2–5.1 s) (Fig. 6*A*,*B*), consistent with the time course of Ca^{2+}–CaM-mediated inhibition of the SAG conductance (Fig. 1).

The extent of adaptation as derived from the ratio (r) between plateau and peak amplitudes (r value) was 0.48 ± 0.05 ($n = 8$; range: 0.2–0.64). We obtained very similar results when we used single ligands such as 2-heptanone ($n = 18$) or the major histocompatibility complex class I peptide SYFPEITHI ($n = 7$) (Fig. 6*D–F*). This decrease in the amplitude of pheromone-evoked potentials during sustained or repetitive stimulation shows that VSNs possess effective regulatory mechanisms that adjust the gain and amplification of the signal transduction machinery in a time-dependent manner after chemostimulation.

Ca^{2+}–CaM-dependent feedback inhibition would be ideally suited to mediate sensitivity regulation in VSNs. We disrupted the CaM feedback by applying ophiobolin A (100 μM, 10 min pretreatment) to the VNO neuroepithelium. In the presence of the CaM antagonist, adaptation was virtually absent, as indicated by the loss of the progressive reduction of the field potential response during chemostimulation (Fig. 6*D–F*) ($n = 20$). Furthermore, the size of responses to the first and second stimuli were nearly identical with ophiobolin A (Fig. 6*D*,*E*) ($n = 20$). To test for any nonspecific effects of ophiobolin A on other membrane-associated components of the transduction cascade, we compared field potential peak response (Fig. 6*G*), time-to-peak (Fig. 6*H*) as well as response delay and slope of the initial rising phase (Fig. 6*I*,*J*) in control ($n = 15$) and ophiobolin A-treated ($n = 20$) VNOs. There were no systematic differences, indicating that ophiobolin A treatment did not alter the molecular steps upstream from the pheromone-sensitive channels.

If this CaM-mediated adaptation depends on Ca^{2+} entry through pheromone-sensitive ion channels, lowering the extracellular Ca^{2+} concentration in the solution surrounding the VSN microvilli and dendritic knobs should decrease the extent of adaptation and thus mimic the effect of CaM antagonists. This was indeed the case, as shown by the collective results of Figure 6*K* [$n = 13$; stimuli: 2,5-dimethylpyrazine (10 nM), 2-heptanone (10 nM), or farnesene (10 nM)]. Hence, removal of the Ca^{2+}–CaM feedback, by preventing Ca^{2+} entry through transduction channels or by functional blockade of intracellular CaM signaling, minimizes or eliminates VSN adaptation. Because the tight junctions sealing off the luminal side of the sensory epithelium are still intact in this preparation, the low Ca^{2+} concentration will only

be "sensed" by the microvilli and the knob, not the dendrite, soma or axon of a given VSN. These results, therefore, strongly implicate the transduction channels in the microvilli and knob as the source of Ca^{2+} entry mediating adaptation. Subsequent voltage-clamp experiments shown in the following (Fig. 7*A*,*B*) support this conclusion.

Ca^{2+}–CaM-dependent adaptation modulates pheromone responsivity of individual VSNs

To validate the findings obtained from the analysis of population responses, we next investigated pheromone-evoked sensory currents in individual, voltage-clamped VSNs that were maintained in acute VNO tissue slices [holding potential, −70 mV; DU, 1:100]. For these experiments, we used a paired-pulse protocol in which two identical 20 s pulses were separated by a 30 s rest period (Fig. 7*A*,*B*). The first stimulus evoked a sensory current that rose to a peak and then declined back to a steady plateau, despite the continued presence of the chemostimulus ($n = 10$). This adaptation occurred with an onset time constant of 2.4 ± 0.6 s ($n = 10$). The extent of adaptation, as derived from the *r* value, was 0.2 ± 0.04 under these conditions ($n = 10$). In contrast, the second pulse evoked a strongly diminished response similar in size to the plateau current of the first response (Fig. 7*A*) ($n = 7$). No further adaptation occurred during the second stimulus (Fig. 7*A*,*B*), indicating that the first (conditioning) response had fully adapted the cells. These results recapitulate the findings obtained from population responses as shown in Figure 6 and thus directly demonstrate that primary sensory currents in VSNs undergo time-dependent adaptation in response to chemostimulation. The data also show that VSNs do not recover from this adaptation during the 30 s interpulse interval (Fig. 7*A*), although recovery eventually did occur after washing periods of several minutes (data not shown). Importantly, these results also provide some insight into the potential source of Ca^{2+} entry underlying adaptation and thus support the findings of Figure 6*K*. For example, VSNs not only express Ca^{2+}-permeable TRPC2 channels but also a variety of voltage-gated Ca^{2+} channels (Liman and Corey, 1996; Ukhanov et al., 2007). Under the voltage-clamp conditions used here (Fig. 7*A*,*B*), activation of voltage-gated Ca^{2+} channels is prevented. Hence, we conclude that localized Ca^{2+} entry through transduction channels but not voltage-gated Ca^{2+} channels is essential for paired-pulse adaptation in single VSNs.

Thus far, our findings indicate that VSNs exhibit efficient adaptation mechanisms that modulate the gain of signal transduction and thus alter the sensitivity of a VSN to a given stimulus. Next, we used current-clamp recordings from individual VSNs in tissue slices to determine, whether adaptation affects the output signal of a given VSN to alter the information that would be transmitted to the accessory olfactory bulb (Fig. 7*C*–*N*). These experiments used the same paired-pulse paradigm as in Figure 7*A*. Consistent with the voltage-clamp experiments, we found that the first stimulus caused a strong reduction in responsivity to the second stimulus, with the average number of action potentials declining from 29 ± 10 ($n = 13$) to 11 ± 5 ($n = 13$) (Fig. 7*C*,*D*). This effect was accompanied by a reduction in the average size of the receptor potential (Fig. 7*E*). No such paired-pulse adaptation was observed when we disrupted CaM signaling with ophiobolin A (100 μM, 10 min pretreatment) (Fig. 7*F*–*H*) ($n = 9$), confirming that this form of adaptation depends on CaM. To test for any nonspecific effects of ophiobolin A, we also used the CaM antagonist CALP2 (50 μM) in single-cell experiments and found that CALP2 abolishes VSN adaptation as well in a manner that is indistinguishable from the ophiobolin A effect (Fig. 7*I*–*L*) ($n = 10$).

To test whether paired-pulse adaptation in current-clamped VSNs involves action potential-dependent Ca^{2+} entry through voltage-gated Ca^{2+} channels, we used current injection to bypass upstream second messenger signaling (Fig. 7*M*,*N*) ($n = 13$). No paired-pulse adaptation was observed under these conditions and neither ophiobolin A nor CALP2 treatment produced significant changes in the number of spikes with current injection (Fig. 7*N*). Thus, paired-pulse VSN adaptation cannot be attributed to Ca^{2+} entry through voltage-gated Ca^{2+} channels, neither in voltage-clamped nor in current-clamped VSNs. Together, the experiments of Figures 6 and 7 provide clear evidence for a role of Ca^{2+} entry and intracellular CaM signaling in VSN adaptation.

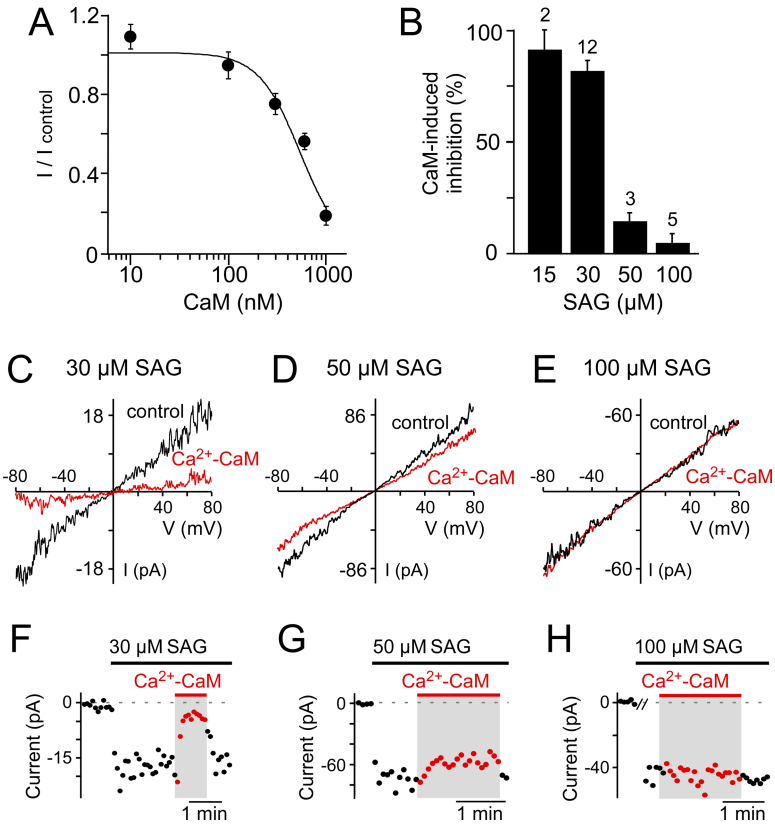

Figure 4. Quantitative analysis of Ca^{2+}–CaM-mediated channel inhibition. ***A***, Dose-dependency of the inhibitory effect of CaM. Each data point consists of 3–8 individual current measurements (at −70 mV). Experiments were done with 50 μM Ca^{2+} to ensure full CaM activation at all concentrations used. ***B***, Histogram showing the dependence of Ca^{2+}–CaM-induced channel inhibition on SAG concentration. Numbers of independent recordings are indicated above each bar. ***C–E***, Examples of *I–V* curves obtained with different concentrations of SAG (30, 50 or 100 μM). The extent of Ca^{2+}–CaM-mediated channel inhibition (red curves; 1 μM CaM, 50 μM Ca^{2+}) differs dramatically, depending on SAG concentration. ***F***, ***G***, Plots showing time courses of the experiments depicted in ***C–E***.

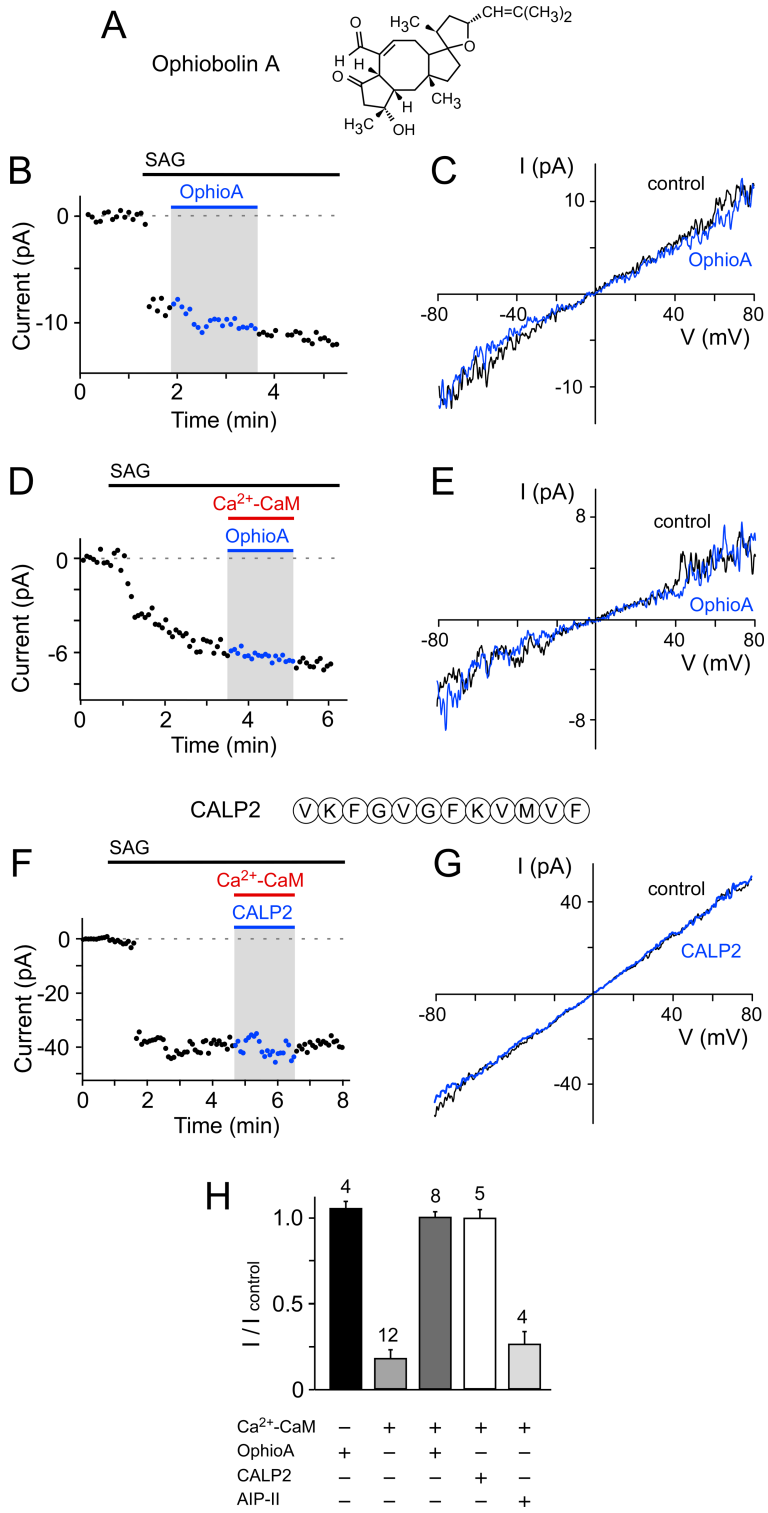

Figure 5. Disruption of Ca^{2+}–CaM-mediated inhibition. ***A***, Chemical structure of the CaM antagonist ophiobolin A. ***B***, ***C***, Ophiobolin A (20 μM, OphioA) applied by itself has no effect on the SAG conductance. ***D***, ***E***, Coapplication of 20 μM OphioA prevents Ca^{2+}–CaM-induced inhibition of SAG currents. ***F***, ***G***, Ca^{2+}–CaM-induced inhibition of SAG currents is prevented by the peptide inhibitor CALP2 (50 μM). ***H***, Summary of the effects of antagonists on Ca^{2+}–CaM-induced inhibition of SAG currents (−70 mV). Each response was normalized to its own control response obtained before application of each test compound. Number of independent recordings indicated above each bar. Note that application of a specific peptide inhibitor of CaMKII, AIP-II (500 nM), does not prevent Ca^{2+}–CaM-mediated channel inhibition.

Discussion

Combined electrophysiological recording of second messenger-evoked ionic currents in excised inside-out membrane patches from VSN dendritic knobs, pheromone-evoked currents and membrane potentials from individual VSNs in VNO tissue slices, and synchronized population responses in intact VNO provided insight into the role of stimulus-induced intracellular Ca^{2+} elevation as a feedback regulator of VSN signaling. Several main findings emerge from this work: (1) the demonstration that VSNs undergo sensory adaptation; (2) the finding that VSN adaptation depends on negative feedback signaling by Ca^{2+} which enters the cell through transduction channels but not voltage-activated Ca^{2+} channels; (3) the demonstration that adaptation is required for modulation of responsivity and sensitivity of stimulus-evoked VSN responses and alters the information transmitted to the brain; (4) the result that activated CaM is required for these effects; (5) the demonstration that pheromone-sensitive TRPC2-dependent cation channels are inhibited by Ca^{2+}–CaM and thus provide a substantial target for a Ca^{2+}–CaM-mediated negative feedback loop; and (6) the demonstration that mouse VSN dendritic knobs express Ca^{2+}-activated cation channels that could be part of an additional, positive feedback mechanism.

Modulation of diacylglycerol-sensitive cation channels by Ca^{2+}–CaM

Ca^{2+}-mediated feedback loops provide important regulatory elements for shaping cellular-signaling responses in space and time (Brandman and Meyer, 2008). In VSNs, receptor activation by a variety of chemosensory ligands generates a transient elevation of intracellular Ca^{2+} that begins in the VSN microvilli and then propagates toward the cell soma (Leinders-Zufall et al., 2000; Cinelli et al., 2002; Spehr et al., 2002; Leinders-Zufall et al., 2004; Chamero et al., 2007; He et al., 2008). Such Ca^{2+} transients are known to depend primarily on Ca^{2+} entry through Ca^{2+}-permeable, TRPC2-dependent cation channels (Lucas et al., 2003; Zufall et al., 2005), although the possibility that a secondary Ca^{2+} release from intracellular stores, as in OSNs (Zufall et al., 2000; Kwon et al., 2009), contributes to Ca^{2+} signaling remains to be tested. The present study identifies native TRPC2-dependent channels as a target for negative feedback regulation by elevated intracellular Ca^{2+}. The inhibitory effect of Ca^{2+} on the pheromone-sensitive channels involves the ubiquitous Ca^{2+} sensor CaM: Ca^{2+}–CaM, but not Ca^{2+} or CaM applied alone, down-regulates channel activation (Fig. 1). This modulatory action of Ca^{2+}–CaM most likely reflects a direct effect on channel gating, since it occurs in the absence of added ATP or GTP, can be abolished by specific CaM inhibitors, and does not require the

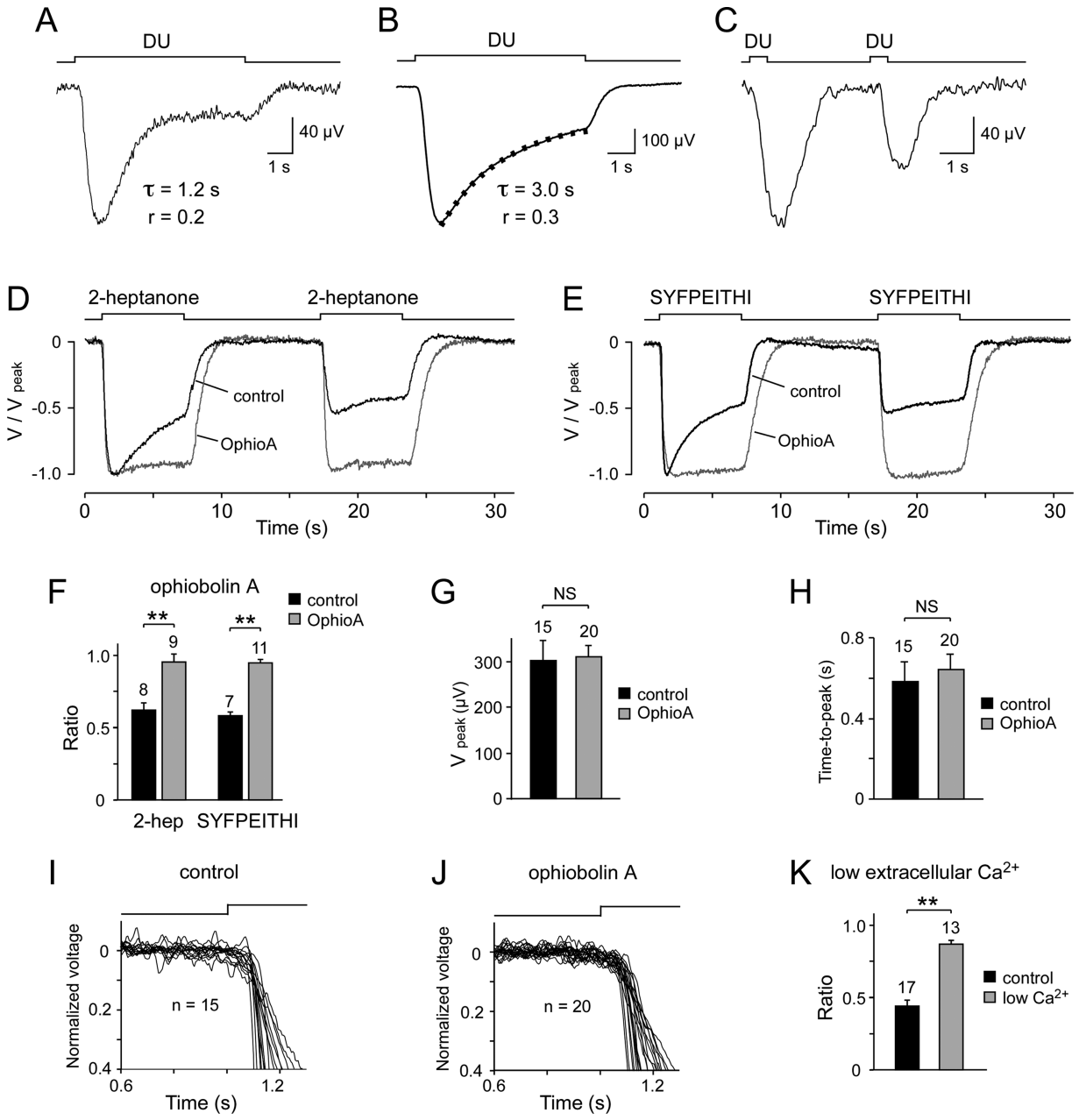

Figure 6. Ca^{2+}–CaM feedback underlies VSN adaptation. ***A–C***, Stimulus-evoked field potentials undergo time-dependent adaptation, evident as a decline of the response during sustained (6 s) stimulation (***A***, ***B***) or as response reduction during brief (500 ms), repetitive stimulation (***C***). Stimulus, DU (1:1000). ***B***, Adaptation onset time course obtained from a single exponential fit (Levenberg-Marquardt nonlinear, least-squares algorithm) of the desensitization phase superimposed on the voltage trace (dotted line). Time constants (τ) are indicated. To quantify the extent of adaptation, the ratio (r) between plateau and peak amplitudes (r value) is given in (***A***, ***B***, ***F***, ***K***). ***D–J***, Comparison of stimulus-induced VNO responses under control conditions (black) and in the presence of ophiobolin A (100 μM; gray). Responses were scaled to enable direct comparison of adaption time courses in different experiments. Two identical 6 s pulses of 10 nM 2-heptanone (***D***) or 0.3 pM SYFPEITHI (***E***), respectively, were applied. Interpulse interval was 10 s. Note that ophiobolin A treatment abolishes sensory adaptation. ***F***, Quantitative analysis of the effect of ophiobolin A on adaptation. Control (black), ophiobolin A (gray). r values of the first response are shown. For stimulation with 2-heptanone, $r = 0.62 \pm 0.04$ for control and $r = 0.95 \pm 0.02$ for ophiobolin A; for stimulation with SYFPEITHI, $r = 0.58 \pm 0.04$ for control and $r = 0.94 \pm 0.02$ for ophiobolin A (**LSD: $p < 0.0001$). Number of independent recordings indicated above each bar. ***G***, Lack of effect of ophiobolin A on the size of the peak response. For control (black), $V_{peak} = 300.8 \pm 45.3$ μV; for ophiobolin A (gray), $V_{peak} = 311.4 \pm 21.0$ μV (NS; t test: $p = 0.82$). ***H***, Time-to-peak values of control and ophiobolin A-treated field responses do not differ significantly. For control (black), time-to-peak $= 0.58 \pm 0.10$ s; for ophiobolin A (gray), time-to-peak $= 0.64 \pm 0.07$ s (NS; t test: $p = 0.62$). Number of independent recordings indicated above each bar. Stimuli were 2-heptanone (10 nM) or SYFPEITHI (0.3 pM). ***I***, ***J***, Plot of the initial rising phase of control (***I***) and ophiobolin A-treated (***J***) field responses. No systematic difference in response delay or slope of the initial rising phase is observed. ***K***, VSN adaptation requires Ca^{2+} entry. Comparison of r values of field potentials with normal (1 mM; control, black) or lowered extracellular Ca^{2+} (0.9 μM; low Ca^{2+}, gray). For control, $r = 0.44 \pm 0.03$; for low Ca^{2+}, $r = 0.86 \pm 0.02$ (**t test: $p < 0.0001$). Number of independent measurements indicated above each bar. Stimuli were 2,5-dimethylpyrazine (10 nM), 2-heptanone (10 nM) or farnesene (10 nM). Stimulus duration, 6 s. NS, Nonsignificant.

activity of CaM kinase II (Fig. 5). To support a functional role of CaM in primary signal transduction of VSNs, we show that CaM colocalizes with TRPC2 in VSN microvilli (Fig. 3).

In addition to this negative feedback loop, positive feedback by Ca^{2+} signaling is likely to occur in VSNs as well. The results of Figure 2 demonstrate a CAN channel in excised membrane patches from dendritic knobs of VSNs, consistent with previous findings in hamster VSNs (Liman, 2003). Hence, the TRPC2-

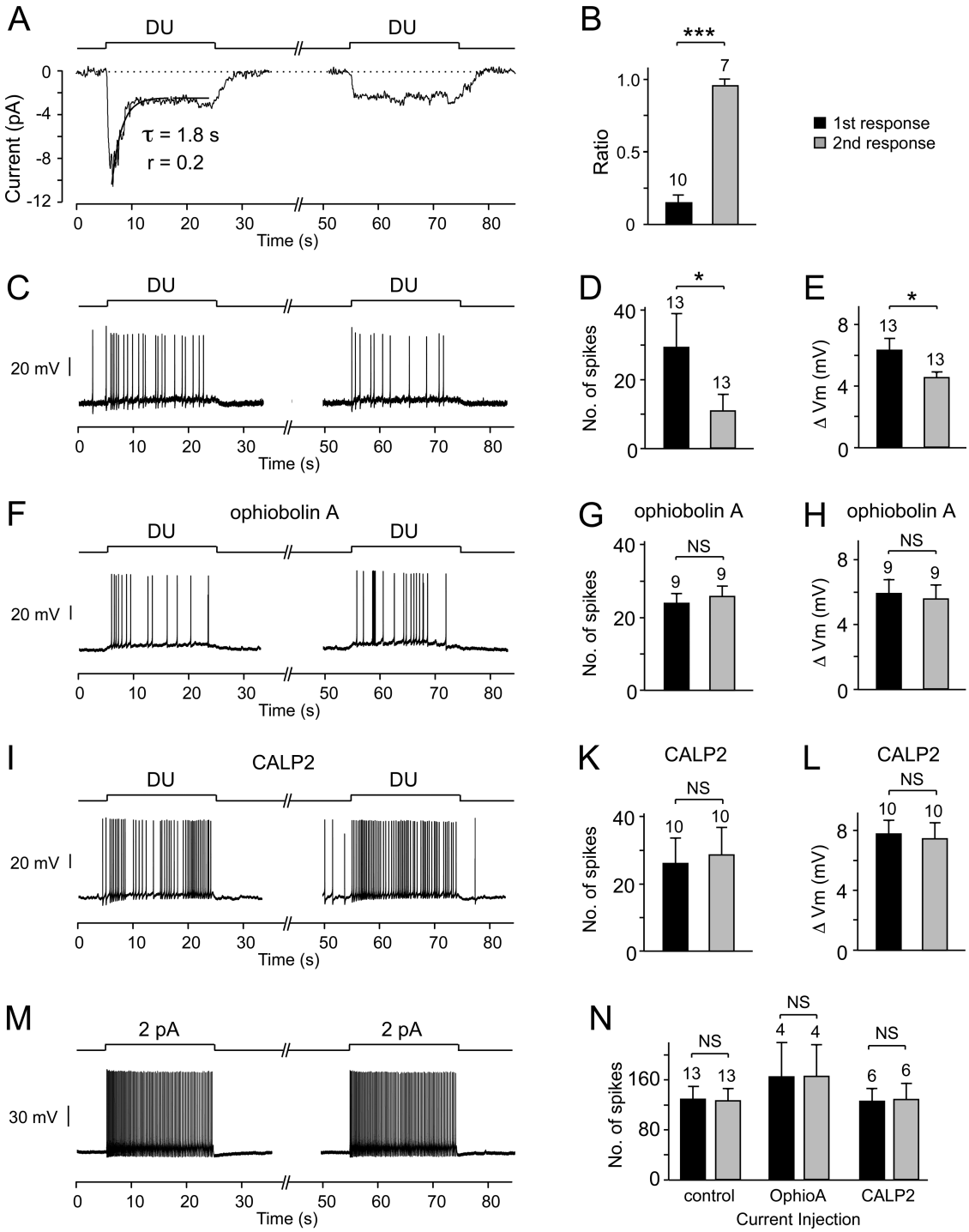

Figure 7. Evidence for Ca^{2+}–CaM-mediated adaptation in individual VSNs. ***A***, Paired-pulse stimulation using two identical 20 s stimuli separated by a 30 s rest period (1:100, DU) reveals adaptation of primary sensory currents in voltage-clamped VSNs. Membrane potential, −70 mV. A single exponential fit of the onset phase of adaptation is superimposed on the current trace to the first stimulus. ***B***, Extent of adaptation as measured by the ratio between plateau and peak currents (***t test: $p < 0.0001$). ***C–E***, Paired-pulse adaptation in single current-clamped VSNs (DU, 1:100). Less neural activity is produced by the second stimulus presentation, as derived from the number of spikes per 20 s stimulation period (***D***) or the mean amplitude of the receptor potential (***E***) (*t test: $p < 0.05$). ***F–L***, Such paired-pulse adaptation is abolished after ophiobolin A (***F***, ***G***) or CALP2 (***I–L***) treatment. ***M***, ***N***, Absence of paired-pulse adaptation in response to current injection (2 pA) and lack of effect of ophiobolin A or CALP2 on current-injected VSN responses.

dependent channels are unlikely to be the only target of Ca^{2+} regulation during VSN signal transduction. However, in contrast to the effect of Ca^{2+} on the TRPC2 channel which is inhibitory and thus causes a diminished cellular response, CAN channel activation would further amplify VSN signaling. A second difference between these two channels is in the role of CaM: whereas TRPC2 requires added CaM for Ca^{2+} regulation (Fig. 1), the CAN channel does not (Liman, 2003; this study) (Fig. 2). Thus, perturbation of CaM signaling as used in this study is unlikely to affect CAN channel function.

Time-dependent adaptation of sensory responses in VSNs

Inhibition of the TRPC2-dependent channels by Ca^{2+}–CaM offers a powerful mechanism for feedback regulation of phero-

mone sensitivity in the VNO. We provide evidence that pheromone-evoked field potentials in intact VNO undergo sensory adaptation, manifested by a time-dependent decline in sensitivity during sustained or repetitive stimulation (Fig. 6). This adaptation arises from the influx of Ca^{2+} and is mediated by CaM. Removal of the Ca^{2+}–CaM feedback, by preventing Ca^{2+} entry or by blockade of CaM signaling, virtually abolishes VSN adaptation (Fig. 6). Such adaptation is also observed at the level of the sensory current in individual, voltage-clamped VSNs maintained in acute VNO tissue slices (Fig. 7). Together, the results of Figures 6 and 7 demonstrate that Ca^{2+}–CaM-dependent adaptation underlies the phasic-tonic responses to pheromone stimulation as observed in this study. Current-clamp recordings demonstrate that Ca^{2+}–CaM feedback effectively regulates the number of action potentials as well as the spiking pattern produced by a given chemostimulus (Fig. 7). This effect cannot be attributed to Ca^{2+} entry through voltage-gated Ca^{2+} channels because (1) the adaptation occurs in voltage-clamped VSNs under conditions that prevent activation of voltage-gated Ca^{2+} channels; and (2) action potential generation produced by current injection, which bypasses upstream second messenger signaling, does not lead to such adaptation (Fig. 7). Analysis of the initial rising phase of field responses argues that blockade of CaM signaling by ophiobolin A does not alter the molecular steps upstream from the pheromone-sensitive channels. Hence, the most likely explanation for the adaptive effect observed here is that it depends on the down-regulation of TRPC2-dependent channels, at least during the onset phase of adaptation.

Comparison with adaptation in OSNs

Our results identify a role of Ca^{2+}–CaM in paired-pulse adaptation of VSNs (Figs. 6, 7). This stands in contrast to OSNs, for which Song et al. (2008) showed that eliminating Ca^{2+}–CaM binding did not affect paired-pulse adaptation, at least via the B1b subunit of the olfactory CNG channel. Another difference between sensory adaptation of OSNs and VSNs is in the recovery time course. Compared with OSNs, recovery from adaptation in VSNs is relatively slow (cf. Munger et al., 2001 and our Fig. 6), occurring on a time scale of minutes. Although the exact mechanisms underlying this sluggish recovery remain to be determined, this finding might explain why previous studies were unable to observe VSN adaptation (Holy et al., 2000; Nodari et al., 2008). For instance, Nodari et al. (2008) typically recorded 100–300 individual stimulus presentations delivered over a period of several hours and defined a VSN response criterion that required a minimum of five trials producing similar sized responses. On the basis of the present results, it seems possible that such responses could have been recorded under conditions in which VSN-signaling cascades were already in a fully adapted state. This would also explain some of the differences in VSN sensitivity between Nodari et al. (2008) and our work.

In the main olfactory epithelium, Ca^{2+}–CaM-mediated adaptation is known to prevent saturation of the signal transduction machinery during background stimulation and thus extends the range of signal detection and discrimination *in vivo* (Kelliher et al., 2003). Ca^{2+}–CaM-dependent regulation of transduction channels might serve a similar function in the VNO. Such a mechanism would make physiological sense, given that (1) activation of the SAG conductance can produce hundreds of picoamperes of inward current, yet only 1–2 pA of current is sufficient to elicit repetitive action potential firing in VSNs, and (2) spike frequency response curves already saturate with inward currents of ~20 pA (Liman and Corey, 1996; Lucas et al., 2003; Shimazaki et al., 2006; Ukhanov et al., 2007). Analysis of the *in vivo* role of VSN adaptation in the context of sensory performance will require genetic manipulation of CaM interactions with the transduction channels, similar to approaches used in the main olfactory epithelium (Munger et al., 2001; Kelliher et al., 2003; Song et al., 2008). However, this goal is not yet feasible in the VNO, mainly because the subunit composition of the native pheromone-sensitive channels is not yet clear (Lucas et al., 2003) and poor expression in heterologous cells makes *in vitro* mutation strategies problematic as well (Hofmann et al., 2002).

Conclusion

It has been thought that the entire chemotransduction process in VSNs fails to adapt (Holy et al., 2000). The observations described in this study are inconsistent with this notion. In fact, our work identifies Ca^{2+}–CaM signaling as a previously unrecognized negative feedback mechanism that tightly adjusts gain and amplification of the chemotransduction process in VSNs. Moreover, we provide evidence for Ca^{2+}–CaM-dependent feedback modulation of native pheromone-sensitive ion channels in the VNO. Finally, our results also suggest the existence of a positive Ca^{2+}-mediated feedback loop in VSNs, through the activation of Ca^{2+}-activated cation channels. These findings should stimulate further studies aimed at understanding how the interaction of negative and positive feedback loops in VSN signal transduction shapes the processing of pheromonal information in the vomeronasal system.

References

Au TK, Chick WS, Leung PC (2000) The biology of ophiobolins. Life Sci 67:733–742.

Brandman O, Meyer T (2008) Feedback loops shape cellular signals in space and time. Science 322:390–395.

Chamero P, Marton TF, Logan DW, Flanagan K, Cruz JR, Saghatelian A, Cravatt BF, Stowers L (2007) Identification of protein pheromones that promote aggressive behaviour. Nature 450:899–902.

Cinelli AR, Wang D, Chen P, Liu W, Halpern M (2002) Calcium transients in the garter snake vomeronasal organ. J Neurophysiol 87:1449–1472.

Del Punta K, Leinders-Zufall T, Rodriguez I, Jukam D, Wysocki CJ, Ogawa S, Zufall F, Mombaerts P (2002) Deficient pheromone responses in mice lacking a cluster of vomeronasal receptor genes. Nature 419:70–74.

He J, Ma L, Kim S, Nakai J, Yu CR (2008) Encoding gender and individual information in the mouse vomeronasal organ. Science 320:535–538.

Hofmann T, Schaefer M, Schultz G, Gudermann T (2002) Subunit composition of mammalian transient receptor potential channels in living cells. Proc Natl Acad Sci U S A 99:7461–7466.

Holy TE, Dulac C, Meister M (2000) Responses of vomeronasal neurons to natural stimuli. Science 289:1569–1572.

Ishida A, Shigeri Y, Tatsu Y, Uegaki K, Kameshita I, Okuno S, Kitani T, Yumoto N, Fujisawa H (1998) Critical amino acid residues of AIP, a highly specific inhibitory peptide of calmodulin-dependent protein kinase II. FEBS Lett 427:115–118.

Kelliher KR, Ziesmann J, Munger SD, Reed RR, Zufall F (2003) Importance of the CNGA4 channel gene for odor discrimination and adaptation in behaving mice. Proc Natl Acad Sci U S A 100:4299–4304.

Kimchi T, Xu J, Dulac C (2007) A functional circuit underlying male sexual behaviour in the female mouse brain. Nature 448:1009–1014.

Kimoto H, Haga S, Sato K, Touhara K (2005) Sex-specific peptides from exocrine glands stimulate mouse vomeronasal sensory neurons. Nature 437:898–901.

Kleene SJ (1994) Inhibition of olfactory cyclic nucleotide-activated current by calmodulin antagonists. Br J Pharmacol 111:469–472.

Kong Au T, Chow Leung P (1998) Identification of the binding and inhibition sites in the calmodulin molecule for ophiobolin A by site-directed mutagenesis. Plant Physiol 118:965–973.

Kwon HJ, Koo JH, Zufall F, Leinders-Zufall T, Margolis FL (2009) Ca^{2+} extrusion by NCX is compromised in olfactory sensory neurons of $OMP^{-/-}$ mice. PLoS ONE 4:e4260.

Leinders-Zufall T, Ma M, Zufall F (1999) Impaired odor adaptation in olfactory receptor neurons after inhibition of Ca^{2+}/calmodulin kinase II. J Neurosci 19:RC19.

Leinders-Zufall T, Lane AP, Puche AC, Ma W, Novotny MV, Shipley MT, Zufall F (2000) Ultrasensitive pheromone detection by mammalian vomeronasal neurons. Nature 405:792–796.

Leinders-Zufall T, Brennan P, Widmayer P, S PC, Maul-Pavicic A, Jäger M, Li XH, Breer H, Zufall F, Boehm T (2004) MHC class I peptides as chemosensory signals in the vomeronasal organ. Science 306:1033–1037.

Leung PC, Taylor WA, Wang JH, Tipton CL (1984) Ophiobolin A. A natural product inhibitor of calmodulin. J Biol Chem 259:2742–2747.

Leypold BG, Yu CR, Leinders-Zufall T, Kim MM, Zufall F, Axel R (2002) Altered sexual and social behaviors in trp2 mutant mice. Proc Natl Acad Sci U S A 99:6376–6381.

Liman ER (2003) Regulation by voltage and adenine nucleotides of a Ca^{2+}-activated cation channel from hamster vomeronasal sensory neurons. J Physiol 548:777–787.

Liman ER, Corey DP (1996) Electrophysiological characterization of chemosensory neurons from the mouse vomeronasal organ. J Neurosci 16:4625–4637.

Liman ER, Corey DP, Dulac C (1999) TRP2: a candidate transduction channel for mammalian pheromone sensory signaling. Proc Natl Acad Sci U S A 96:5791–5796.

Lucas P, Ukhanov K, Leinders-Zufall T, Zufall F (2003) A diacylglycerol-gated cation channel in vomeronasal neuron dendrites is impaired in TRPC2 mutant mice: mechanism of pheromone transduction. Neuron 40:551–561.

Menco BP (2005) The fine-structural distribution of G-protein receptor kinase 3, beta-arrestin-2, Ca^{2+}/calmodulin-dependent protein kinase II and phosphodiesterase PDE1C2, and a Cl^--cotransporter in rodent olfactory epithelia. J Neurocytol 34:11–36.

Menini A (1999) Calcium signalling and regulation in olfactory neurons. Curr Opin Neurobiol 9:419–426.

Meredith M (1983) Sensory physiology of pheromone communication. In: Pheromones and reproduction in mammals (Vandenbergh JG, ed), pp 199–252. New York: Academic.

Munger SD, Lane AP, Zhong H, Leinders-Zufall T, Yau KW, Zufall F, Reed RR (2001) Central role of the CNGA4 channel subunit in Ca^{2+}-calmodulin-dependent odor adaptation. Science 294:2172–2175.

Nodari F, Hsu FF, Fu X, Holekamp TF, Kao LF, Turk J, Holy TE (2008) Sulfated steroids as natural ligands of mouse pheromone-sensing neurons. J Neurosci 28:6407–6418.

O'Connor V, El Far O, Bofill-Cardona E, Nanoff C, Freissmuth M, Karschin A, Airas JM, Betz H, Boehm S (1999) Calmodulin dependence of presynaptic metabotropic glutamate receptor signaling. Science 286:1180–1184.

Peters C, Mayer A (1998) Ca^{2+}/calmodulin signals the completion of docking and triggers a late step of vacuole fusion. Nature 396:575–580.

Potter SM, Zheng C, Koos DS, Feinstein P, Fraser SE, Mombaerts P (2001) Structure and emergence of specific olfactory glomeruli in the mouse. J Neurosci 21:9713–9723.

Shimazaki R, Boccaccio A, Mazzatenta A, Pinato G, Migliore M, Menini A (2006) Electrophysiological properties and modeling of murine vomeronasal sensory neurons in acute slice preparations. Chem Senses 31:425–435.

Song Y, Cygnar KD, Sagdullaev B, Valley M, Hirsh S, Stephan A, Reisert J, Zhao H (2008) Olfactory CNG channel desensitization by Ca^{2+}/CaM via the B1b subunit affects response termination but not sensitivity to recurring stimulation. Neuron 58:374–386.

Spehr M, Hatt H, Wetzel CH (2002) Arachidonic acid plays a role in rat vomeronasal signal transduction. J Neurosci 22:8429–8437.

Stowers L, Holy TE, Meister M, Dulac C, Koentges G (2002) Loss of sex discrimination and male-male aggression in mice deficient for TRP2. Science 295:1493–1500.

Torre V, Ashmore JF, Lamb TD, Menini A (1995) Transduction and adaptation in sensory receptor cells. J Neurosci 15:7757–7768.

Ukhanov K, Leinders-Zufall T, Zufall F (2007) Patch-clamp analysis of gene-targeted vomeronasal neurons expressing a defined V1r or V2r receptor: ionic mechanisms underlying persistent firing. J Neurophysiol 98:2357–2369.

Villain M, Jackson PL, Manion MK, Dong WJ, Su Z, Fassina G, Johnson TM, Sakai TT, Krishna NR, Blalock JE (2000) De novo design of peptides targeted to the EF hands of calmodulin. J Biol Chem 275:2676–2685.

Wysocki CJ, Lepri JJ (1991) Consequences of removing the vomeronasal organ. J Steroid Biochem Molec Biol 39:661–669.

Yildirim E, Dietrich A, Birnbaumer L (2003) The mouse C-type transient receptor potential 2 (TRPC2) channel: alternative splicing and calmodulin binding to its N terminus. Proc Natl Acad Sci U S A 100:2220–2225.

Zufall F, Leinders-Zufall T (2000) The cellular and molecular basis of odor adaptation. Chem Senses 25:473–481.

Zufall F, Leinders-Zufall T, Greer CA (2000) Amplification of odor-induced Ca^{2+} transients by store-operated Ca^{2+} release and its role in olfactory signal transduction. J Neurophysiol 83:501–512.

Zufall F, Ukhanov K, Lucas P, Liman ER, Leinders-Zufall T (2005) Neurobiology of TRPC2: from gene to behavior. Pflugers Arch 451:61–71.